

Magmatic volatile content and the overpressure ‘sweet spot’: Implications for volcanic eruption triggering and style

Anna Brookfield^a, Mike Cassidy^{a,b,*}, Gregor Weber^a, Răzvan-Gabriel Popa^c,
Olivier Bachmann^c, Michael J. Stock^d

^a Department of Earth Sciences, University of Oxford, Oxford, UK

^b School of Geography, Earth and Environmental Science, University of Birmingham, Birmingham, UK

^c Institute of Geochemistry and Petrology, ETH Zürich, Zürich, Switzerland

^d Discipline of Geology, School of Natural Sciences, Trinity College Dublin, Dublin, Ireland

ARTICLE INFO

Keywords:

Overpressure

Volatile content

Timescales

Eruption triggering

ABSTRACT

Volatile exsolution is widely considered to be capable of generating magmatic overpressure and triggering volcanic eruptions. Despite its role as an eruption trigger, exsolution-driven overpressurisation is relatively poorly understood. Part of the problem is that thermodynamic models do not consider how the behaviour of small quantities of magma scales up to reservoir level – where variations in temperature and crystallinity become important. In contrast, many thermomechanical models focus only on magma injection, and do not consider how overpressure evolves spatially or temporally, when related to crystallisation and volatile exsolution. Here, we use Rhyolite-MELTS to track exsolution-driven overpressure during cooling for a variety of natural compositions, storage pressures, initial volatile contents and magmatic X_{H_2O} (molar $H_2O/(CO_2 + H_2O)$). We then couple these outputs to a thermal model to determine the timescales and spatial extent of overpressurisation with varying volatile content.

We find that the highest overpressures occur in magmas which are initially at their H_2O solubility limit, with the addition or removal of H_2O resulting in a decrease in peak overpressure. We also find that maximum overpressure decreases with the addition of CO_2 (decreasing X_{H_2O}) at typical magma storage pressures of 100–230 MPa. The higher overpressures generated at the volatile ‘sweet spot’ have a greater potential to trigger eruptions – or to favour their initiation by making the system more susceptible to other triggers, such as magma injection. The reduction in overpressure with increasing or decreasing initial H_2O suggests that triggering by volatile exsolution is less likely for these magmas. Peak overpressure at the volatile sweet spot also coincides with an increased incidence of explosive eruptions at water contents ~4–5.5 wt%. This suggests that higher magmatic overpressures may produce more explosive eruptions, by driving faster initial ascent rates and decreasing outgassing efficiency in the conduit. Our thermal modelling demonstrates that, for small magmatic systems, exsolution-driven overpressurisation can operate on timescales which are much shorter than the crustal relaxation timescale. In these cases, overpressure cannot be dissipated by a visco-elastic crustal response, and therefore has the potential to trigger a volcanic eruption.

1. Introduction

The presence of a magmatic system within the crust modifies geothermal and lithostatic pressure gradients. Physical and chemical processes operating within a magma reservoir can lead to pressure fluctuations and the build-up of significant overpressures. We define magmatic overpressure (ΔP) as a pressure in excess of the expected lithostatic pressure for a given depth – equivalent to the excess pressure

(p_e) term of Gudmundsson (2012). In some cases, negative overpressure, or underpressurisation, may also occur as a system cools and contracts. Internal overpressurisation may occur via melting, thermal expansion, buoyancy, volatile exsolution, CO_2 -flushing, magma recharge, or a combination of these mechanisms (Cañón-Tapia, 2014; Caricchi et al., 2018). Here, we focus on overpressure generated by volatile exsolution, termed ‘second boiling’ when driven by crystallisation of anhydrous mineral phases. Second boiling has long been considered a viable

* Corresponding author.

E-mail address: m.cassidy.1@bham.ac.uk (M. Cassidy).

<https://doi.org/10.1016/j.jvolgeores.2023.107916>

Received 9 January 2023; Received in revised form 9 September 2023; Accepted 18 September 2023

Available online 4 October 2023

0377-0273/© 2023 The Authors. Published by Elsevier B.V. This is an open access article under the CC BY license (<http://creativecommons.org/licenses/by/4.0/>).

eruption triggering mechanism (Blake, 1984; Tait et al., 1989), and has recently been identified as a potential trigger at Campi Flegrei, Italy (Stock et al., 2016), Kelud, Indonesia (Cassidy et al., 2016, 2019), Mount St Helens, USA (Kent et al., 2007) and Calbuco, Chile (Arzilli et al., 2019).

If overpressure exceeds a threshold value (often termed the ‘critical overpressure’), then magma may ascend towards the Earth’s surface, triggering a volcanic eruption. The critical overpressure (ΔP_c) for a given system is dependent primarily on host rock strength (Pollard, 1987; Rubin, 1995) and is commonly considered to be on the order of tens of MPa (Gudmundsson, 2012). However, it is debated that (ΔP_c) may be higher than this, on the order of ~ 100 MPa, and is particularly sensitive to pore fluid pressure (Grosfils et al., 2015; Albino et al., 2018). The timescale of overpressure build-up is also important for determining whether a volcanic eruption will occur. For exsolution-driven overpressurisation, two important timescales have been identified: 1. the crustal relaxation timescale (τ_{relax}), and 2. the cooling timescale (τ_{cool}) (Degruyter and Huber, 2014). If $\tau_{\text{relax}} < \tau_{\text{cool}}$ then overpressure can be dissipated by the surrounding crust, and an eruption is unlikely. However, if $\tau_{\text{cool}} < \tau_{\text{relax}}$, overpressure cannot be dissipated by viscous crustal behaviour, and could potentially trigger an eruption by brittle failure of the reservoir wall.

In addition to its role in triggering volcanic eruptions, magmatic overpressure is thought to be linked to eruption style (Jaupart and Allègre, 1991; Woods and Koyaguchi, 1994), most likely via its control on magma ascent rate and outgassing efficiency (Cassidy et al., 2018). One factor influencing both overpressure and ascent rate is magmatic volatile content. Water-rich magmas are often associated with explosive eruptions (Papale et al., 1998; Cashman, 2004; Gonnermann and Manga, 2012) due to the volumetric expansion and increased buoyancy associated with volatile-exsolution in the conduit, and also the effect of volatiles on increasing magma ascent rate, allowing less time for degassing prior to eruption. However, there is also evidence for effusive, water-saturated eruptions at Volcan Quizapu (Ruprecht and Bachmann, 2010) and Nisyros and Yali volcanoes (Popa et al., 2019, 2021a); hence, magmas stored in the presence of exsolved volatiles can be associated with both explosive and effusive activity. A key question, therefore, is: what are the volatile conditions within a magma reservoir (both dissolved and exsolved), that promote either effusive or explosive eruptions?

Our ability to conceptualise exsolution-driven overpressurisation is hampered by a lack of integration between different types of models. Thermodynamic models can describe the equilibrium chemical state of a magmatic system as it cools, but do not incorporate important physical factors such as reservoir size, shape or the properties of the surrounding crust. In contrast, thermomechanical models often assume instantaneous and homogenous pressurization, and tend to focus on magma injection as the pressurising mechanism, rather than second boiling. Additionally, the temperature within a cooling reservoir will vary with proximity to the surrounding crust, resulting in variations in crystallinity and the amount of volatile exsolution throughout the reservoir. By coupling thermodynamic and thermal models we provide a first-order method for determining changes in pressurization induced by cooling and crystallisation. This represents a step forward in that we model temporal and spatial changes in overpressure connected to evolving physical parameters, rather than assuming instantaneous, homogenous overpressure throughout the whole reservoir.

In this study we aim to answer key questions such as; How does overpressure evolve throughout a magma reservoir as a whole, with areas of varying temperature, and therefore varying amounts of volatile exsolution? How do variations in fluid content affect overpressurisation? How does overpressure vary spatially as different parts of the reservoir reach high crystallinities? Can this type of overpressure (volatile exsolution-driven) accumulate on timescales rapid enough to trigger an eruption? And finally, do these internal pressurization processes have any effect on eruption style?

2. Methods

2.1. Rhyolite-MELTS thermodynamic modelling

To investigate the overpressure evolution of magma during cooling we use Rhyolite-MELTS thermodynamic modelling software, version 1.2 (Gualda et al., 2012; Ghiorso and Gualda, 2015; Gualda and Ghiorso, 2015). We model the following volcanic systems: Nisyros-Yali dacite (Greece), Calbuco basaltic andesite (Chile), Kelud basaltic andesite (Indonesia) and Mount St Helens dacite (USA) – all of which have shown a variety of eruption styles. Magma composition, pressure, temperature and fluid inputs for these simulations are shown in Table S1, and melt composition plots are shown in Fig. S1. Although these systems all have relatively well-constrained storage conditions, these parameters are often debated as research progresses. Therefore, we seek to present general trends in overpressurisation with varying fluid content, rather than replicate exactly the conditions for each system. This is also true of the ability of melts to replicate exactly the evolution of a given system. As shown in Fig. S1 there are discrepancies between our modelled liquid lines of descent and observed geochemistry, so we discuss general trends in overpressurisation, rather than attempt to discuss the overpressure evolution of a particular system in detail.

We run isobaric cooling simulations for each of the four volcanic systems at 2 °C temperature increments, starting at the liquidus, for two sets of simulations:

- 1) A set of three simulations with varying initial H₂O contents which are CO₂-free.
- 2) A set of three simulations with varying proportions of H₂O and CO₂ ($X_{\text{H}_2\text{O}} = (\text{H}_2\text{O} + \text{CO}_2)/\text{H}_2\text{O}$).

For set 1, H₂O solubility is determined in Rhyolite-MELTS by incrementally increasing H₂O content at the liquidus temperature, for a fixed pressure and composition (Table S1) until a fluid phase exsolves. We then add or subtract H₂O at the same pressure, adjusting the temperature to the new liquidus value. In this way, we can compare the effect of initial H₂O- undersaturation and oversaturation with simulations where H₂O content is at the solubility limit, where all simulations begin at the liquidus temperature. For set 2, the simulation at water saturation is used as the $X_{\text{H}_2\text{O}} = 1$ case, and $X_{\text{H}_2\text{O}}$ is then decreased at a fixed total fluid content through the addition of CO₂. We note that starting our simulations at the same temperature (rather than adjusting to the liquidus) still results in the same trends in overpressure described in the results section. Outputs from the Rhyolite-MELTS cooling simulations are used to calculate magmatic overpressure at each temperature increment, following the method of Tramontano et al. (2017):

$$\Delta P = \Delta V / (V^* \beta) \quad (1)$$

Where ΔP is magmatic overpressure (MPa), ΔV is potential volume change relative to initial volume at the liquidus (m^3), V is system volume (m^3) and β is system compressibility ($1/\text{MPa}$). The β output is calculated in MELTS as the sum of the liquid, crystal and fluid compressibilities, multiplied by the respective volume fraction of each phase. For the systems investigated here, Rhyolite-MELTS generates β values on the order of 10^{-9} to 10^{-11} Pa^{-1} . These values are consistent with multiple independent estimates of magma compressibility from numerical modelling (Huppert and Woods, 2002 [10^{-8} to 10^{-10} Pa^{-1}]), ground deformation studies (Gottsmann and Odbert, 2014 [1×10^{-9} - $4 \times 10^{-11} \text{ Pa}^{-1}$]), and multidisciplinary constraints (Wasser et al., 2021 [$\sim 3.8 \times 10^{-10} \text{ Pa}^{-1}$]).

In our thermodynamic modelling we envisage that magma generated at greater depths has different initial volatile contents. As the magma ascends from the lower to the upper crust, these volatiles will exsolve during decompression (first boiling), and some will be outgassed. By the time they reach the upper crust where most magma reservoirs stall and

reside (Huber et al., 2019) some magmas will be H₂O-undersaturated, saturated or even oversaturated and this is where we begin our simulations. Although there are cases where first boiling drives supersaturated magma from the lower crust all the way to the surface (Ruprecht and Plank, 2013), we assume that supersaturated magma can stall in the mid-upper crust (e.g., (Annen et al., 2006; Kent et al., 2010; Ruprecht and Plank, 2013; Rasmussen et al., 2022)). In all of our simulations we assume that the melt and exsolved volatile phase remain coupled. For the majority of our calculations (Figs. 1 to 6) we assume closed-system conditions where exsolved volatiles are not lost via outgassing, and so these overpressures are likely to represent maximum values. However, in section 5.2 we also quantify the effect of open-system degassing on overpressure generation. Implicit in the isobaric cooling calculations is the assumption that the crust surrounding the magma reservoir is rigid, and so does not dissipate any of the pressure caused by volume increase. This is the same as assuming that the timescale for cooling, crystallisation and volatile exsolution is shorter than the timescale of crustal relaxation. Based on the overpressure timescales for a generic, shallow

reservoir reported here, and typical crustal relaxation timescales discussed below, this assumption is valid for small reservoirs at relatively shallow depths. However, the assumption may not hold for larger, deeper reservoirs, which have longer cooling timescales. This method does not account for the effect of changes in pressure on volatile solubility. As stated in Tramontano et al. (2017), this is a valid assumption for overpressures $\lesssim 25$ MPa, but may have effects for overpressures larger than this. Model limitations and their implications for our findings are discussed further in section 5. Nevertheless, our method still provides a useful way of comparing relative magnitudes of overpressure with varying fluid content, and timescales to reach critical overpressure.

2.2. Thermal modelling

To determine the timescales of pressurization from cooling and volatile exsolution, we input melt fraction and overpressure outputs from Rhyolite-MELTS into a thermal model (Weber et al., 2020). We use a 2.5-dimensional, axisymmetric cylindrical model to simulate magma

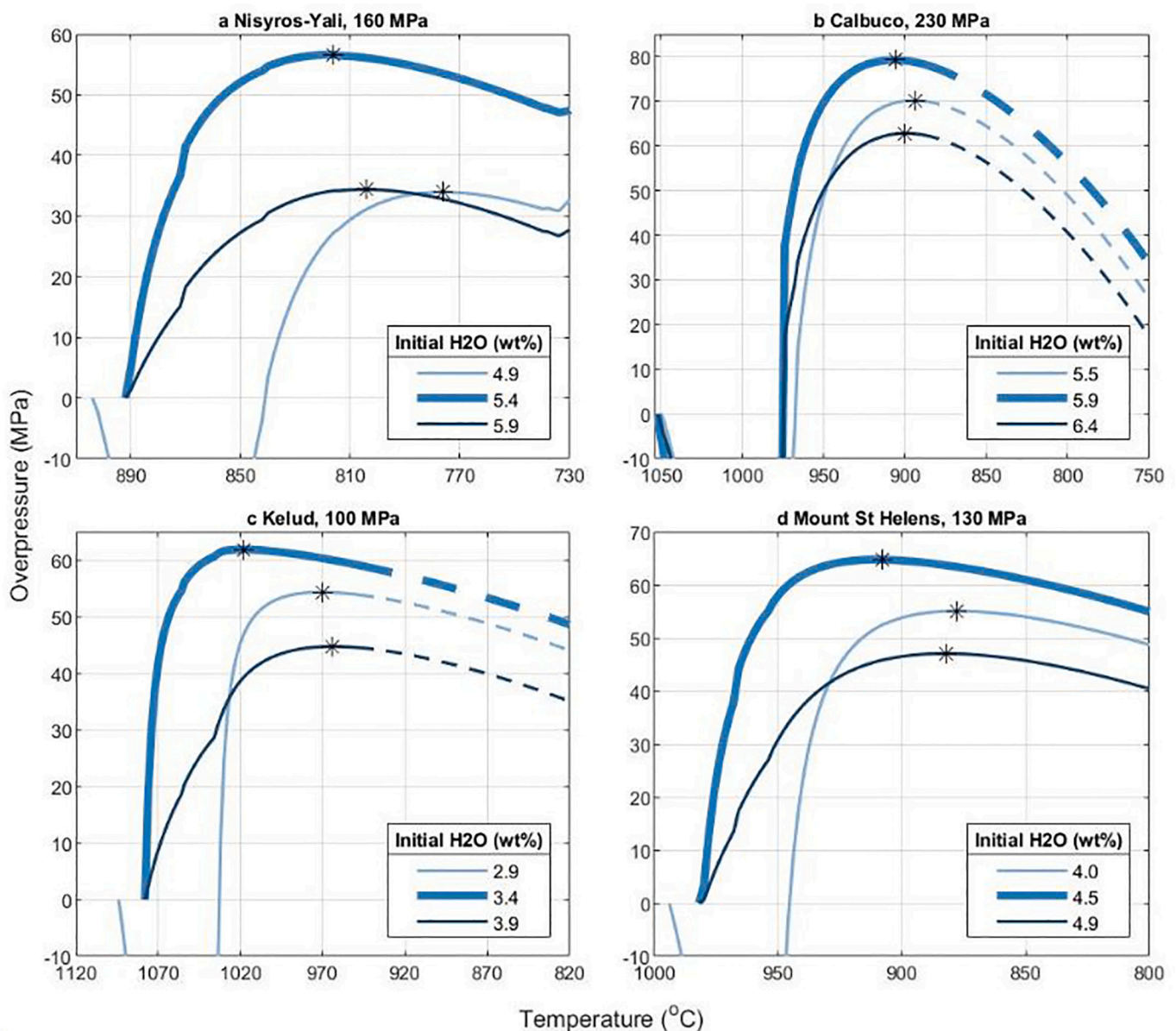


Fig. 1. Overpressure evolution for varying volcanic systems calculated from Rhyolite-MELTS for varying initial H₂O content, no CO₂. All simulations begin at the liquidus, and overpressure is calculated relative to the liquidus. Stars indicate peak overpressure. Dashed lines indicate crystallinity > 60 vol%. Thicker lines indicate simulations which are initially at the H₂O solubility limit.

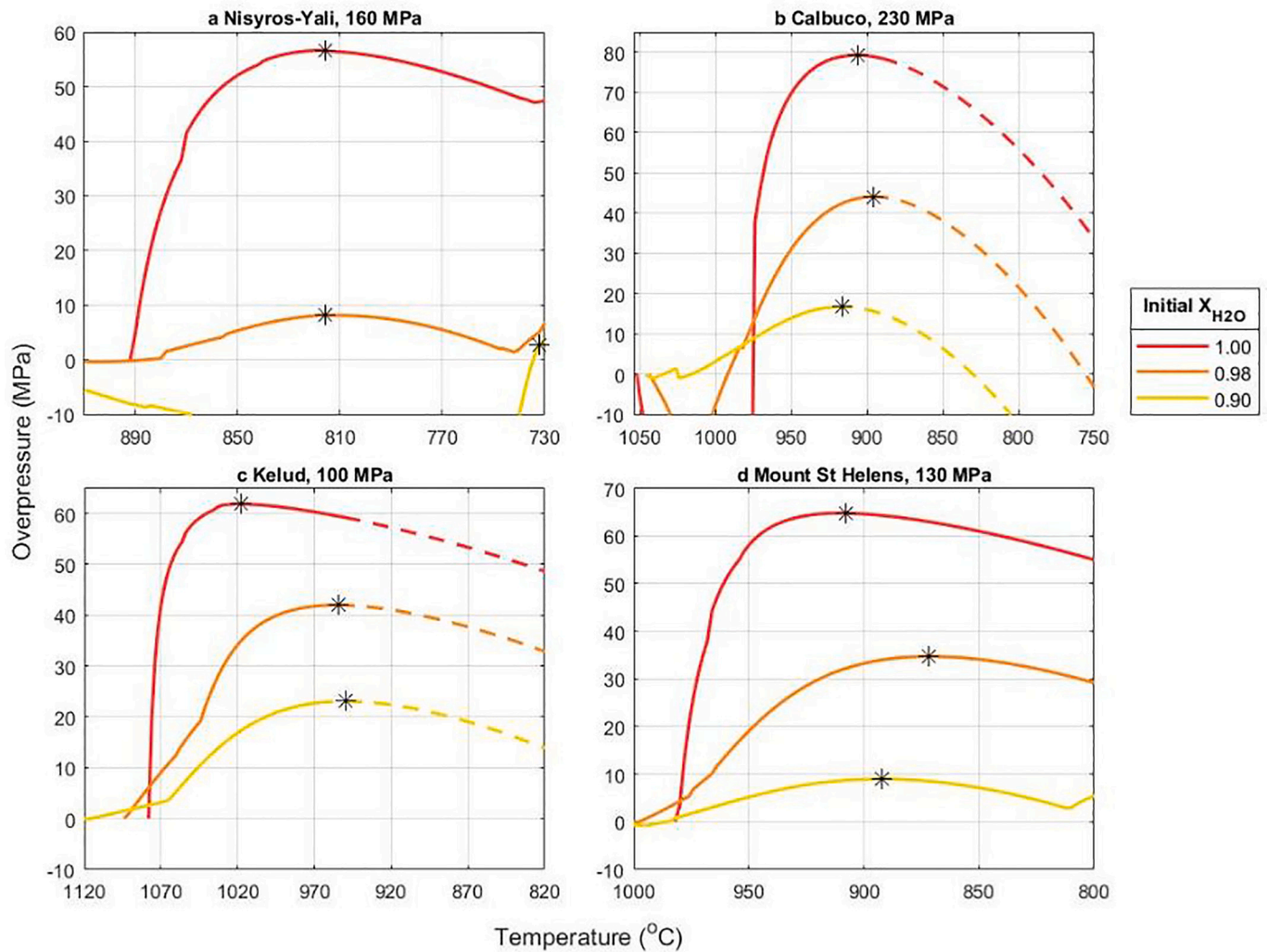


Fig. 2. Overpressure evolution for varying volcanic systems calculated from Rhyolite-MELTS for varying initial X_{H_2O} . All simulations begin at the liquidus, and overpressure is calculated relative to the liquidus. Stars indicate peak overpressure. Dashed lines indicate crystallinity > 60 vol%.

reservoir cooling via conductive heat transfer. We use an initial geothermal gradient of 25 °C/km, a thermal conductivity of 2.3 W/m/K, a density of 2700 kg/m³, a latent heat of 320,000 J/kg and a specific heat of 1050 J/Kg/K. These values are within the range of those used in other studies (e.g. [Whittington et al., 2009](#); [Degruyter and Huber, 2014](#); [Trasatti et al., 2019](#)) and are broadly applicable to magma stored at shallow to mid-crustal levels. We model a cylindrical magma body with a top surface at 4 km depth, representing shallow crustal storage towards the upper boundary of common storage depths for intermediate arc magmas ([Rasmussen et al., 2022](#)). To present a generically applicable case, reservoir height and radius are both fixed at 1 km, representing a total volume of 3.14 km³. This represents a relatively small reservoir, and is in line with volumes considered in other studies ([Odbert et al., 2014](#); [Albino et al., 2018](#); [Forni et al., 2018](#)). Melt fraction and temperature data from Rhyolite-MELTS outputs are used to implement latent heat of crystallisation by fitting a polynomial curve to these data (Fig. S2). We use outputs for the Kelud volcanic system (basaltic andesite) here, but our method could be applied to any other system of interest. The thermal model uses a finite difference method to solve the axisymmetric formulation of the heat conduction equation. To extract variations in overpressure as the reservoir cools, we track the temperature in numerical cells and link this to overpressure via the overpressure-temperature relationship derived from the Rhyolite-MELTS calculations. We present weighted average overpressure values for the whole reservoir over time (weighted by volume), assuming an

average lithostatic reservoir pressure of 100 MPa (Table S1). To distinguish between the average overpressures from our thermal modelling and those derived from Rhyolite-MELTS (which are relevant for a homogeneous system), we refer to the thermal model-derived overpressures as ‘average reservoir overpressure’.

Using average overpressure values assumes that the magma can transfer stress evenly throughout its volume, an assumption which may not be valid for mushy, heterogeneous reservoirs. However [Parmigiani et al. \(2017\)](#) show that the random distribution of bubbles associated with volatile-exsolution hinders the development of pore-scale degassing pathways in a reservoir. As pressurization from volatile-exsolution is likely to be distributed throughout the reservoir, average pressurization may be the best way to model this complex process. Our model does not account for the movement of volatiles through the magma reservoir ([Annen and Burgisser, 2021](#)), or the effect of buoyancy in generating overpressure ([Caricchi et al., 2014](#)). The importance of the buoyancy effect on reservoir overpressurisation will depend on the timescales of bubble rise relative to volatile exsolution ([Pyle and Pyle, 1995](#)). Although we discuss overpressure as an eruption trigger, we do not consider the location of fracturing within the reservoir, or the progress of fracturing once critical overpressure has been reached. A review of fracturing and dyke propagation is given in ([Rivalta et al., 2015](#)), and ([Gregg et al., 2012](#)) discuss how and where the crust is likely to fail in response to overpressurisation. We also note that our thermal model only accounts for heat transfer via conduction, it does not incorporate

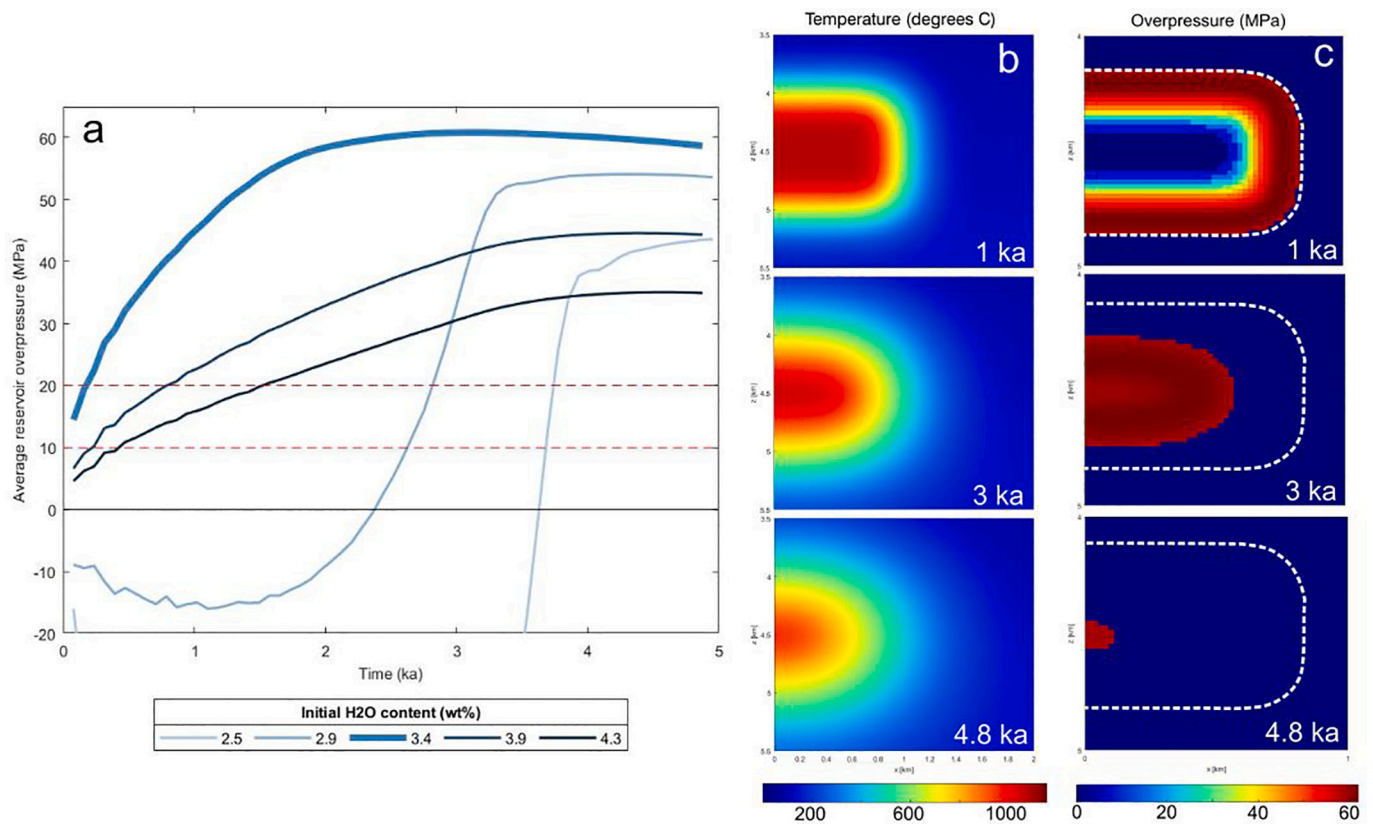


Fig. 3. Temporal evolution of average reservoir overpressure for varying initial H₂O content. a) Overpressure evolution for Kelud at 4 km reservoir depth. Thermal model uses a 1×1 km reservoir (3.14 km^3 volume) and the simulations are truncated at 60% crystallinity. Red dashed lines highlight 10 and 20 MPa overpressure thresholds (see discussion). b) Thermal model outputs showing temperature variations for the 3.4 wt% H₂O case after 1 ka, 3 ka and 4.8 ka. c) Thermal model outputs showing overpressure variations for the same case. White dashed line shows extent of magma reservoir at 1 ka. Blue space within this outline at 3 ka and 4.8 ka represents uneruptible magma. (For interpretation of the references to colour in this figure legend, the reader is referred to the web version of this article.)

convection or advection. It has been shown that convective heat transfer via a hydrothermal system can increase cooling rates by orders of magnitude (Kelly et al., 2021). Therefore, the timescales presented here are upper estimates, and cooling rates are likely to be shorter in natural systems, assuming no magmatic recharge.

3. Modelling results

3.1. Thermodynamic modelling

3.1.1. Effect of varying initial H₂O content (no CO₂)

The evolution of magmatic overpressure during cooling for the four different systems investigated here is shown in Fig. 1. Initial H₂O content is varied, and there is no CO₂ present in these simulations. We use a crystallinity cut-off of 60 vol% (dashed lines on plots denote >60% crystallinity) to separate eruptible from non-eruptible magmas (Cooper and Kent, 2014) although, in some cases, it may be possible to exceed this limit and erupt (Klein et al., 2017). In agreement with Tramontano et al. (2017), we find that maximum overpressures are attained when initial H₂O concentrations are set at their solubility limit (thicker lines in figures). However, we also find that increasing the initial H₂O concentration above the solubility limit results in a decrease in peak overpressure for all our modelled systems. For example, at Nisyros-Yali (Fig. 1a) the simulation initiated at the H₂O solubility limit (5.4 wt%) generates a peak overpressure of 56 MPa, whereas reducing the H₂O concentration to 4.9 wt% (i.e. water undersaturation) and increasing it to 5.9 wt% (water oversaturation) both lower the peak overpressure to 33 MPa and 34 MPa, respectively. Similar trends in overpressure are seen consistently across all the systems that we model (Fig. 1b-d),

suggesting that the reduction in overpressure with increasing or decreasing initial H₂O content occurs regardless of storage depth, temperature or magma composition. This trend in overpressure with varying initial H₂O content is also apparent at smaller H₂O increments of 0.05 wt% (Fig. S3), and for basaltic and rhyolitic compositional end-members (Fig. S4). Simulations with initial H₂O concentrations at the solubility limit have the maximum potential for volume change (ΔV), without the dampening effect (increased compressibility (β)) of excess exsolved volatiles. The addition or removal of H₂O shifts this balance and reduces overpressure. Hence, initial H₂O contents at the water solubility limit result in a ‘sweet spot’ where magmas generate maximum peak overpressure. The eventual decline in overpressure seen across all systems - and all initial water contents - is due to the effect of crystallisation and liquid contraction during cooling which both decrease system volume, and also the effect of continued fluid exsolution, which increases system compressibility.

3.1.2. Effect of varying $X_{\text{H}_2\text{O}}$ (adding CO₂)

We modelled each volcanic system with varying $X_{\text{H}_2\text{O}}$ from 0.9 to 1 by adding a CO₂ phase, to investigate the effect of mixed volatile exsolution on the generation of overpressure (Fig. 2). The simulations initially at the water solubility limit (thicker lines in Fig. 1) are used as the $X_{\text{H}_2\text{O}} = 1$ case, and total fluids are fixed at this value. Our results indicate that the highest overpressures occur in pure-H₂O systems ($X_{\text{H}_2\text{O}} = 1$), with overpressure decreasing as $X_{\text{H}_2\text{O}}$ decreases. For example, a maximum overpressure of 62 MPa is attained at Kelud in the $X_{\text{H}_2\text{O}} = 1$ simulation (Fig. 2c). As $X_{\text{H}_2\text{O}}$ decreases with the addition of CO₂, peak overpressure decreases to 42 MPa for $X_{\text{H}_2\text{O}} = 0.98$, and 23 MPa for $X_{\text{H}_2\text{O}} = 0.80$. The same trend is seen across all the volcanic systems modelled

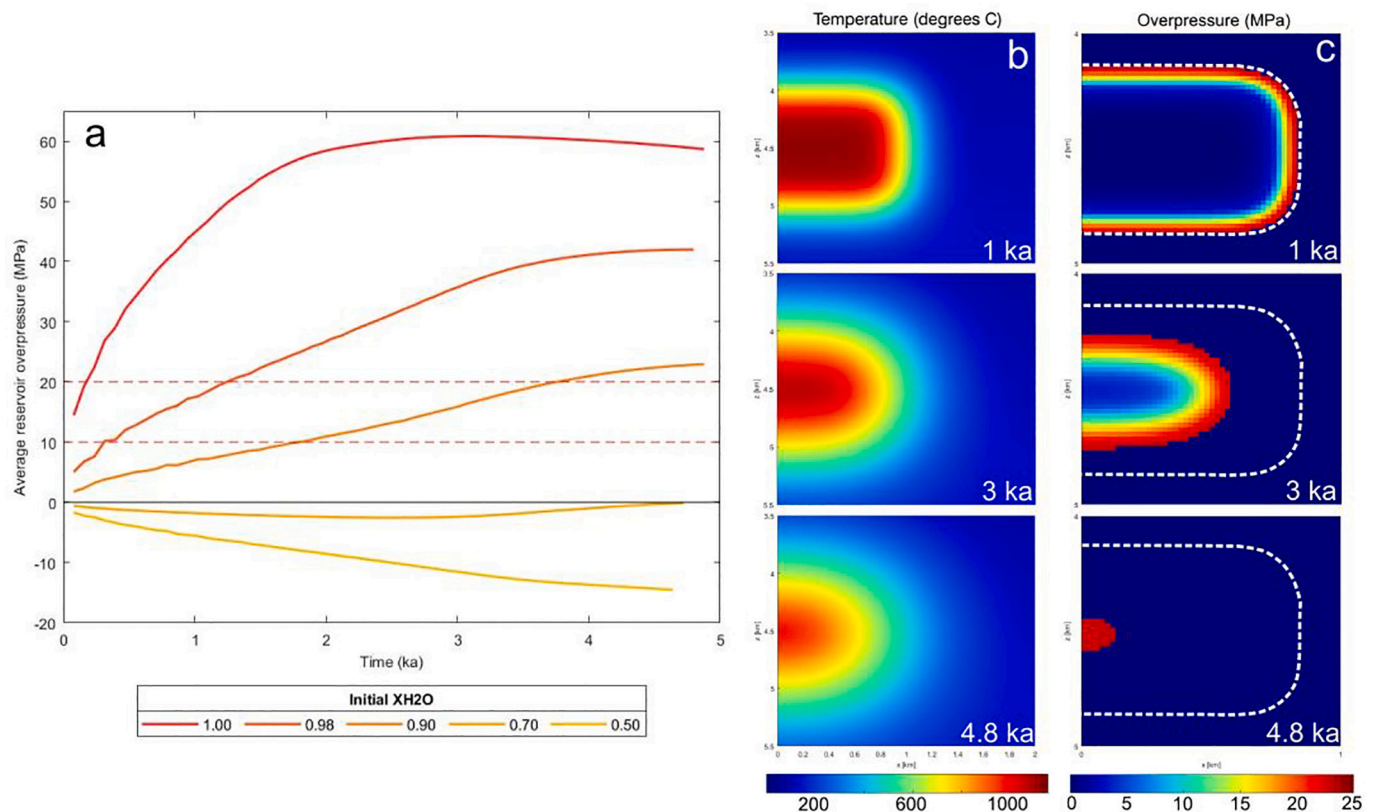


Fig. 4. Temporal evolution of average reservoir overpressure for varying initial X_{H_2O} . a) Overpressure evolution for Kelud at 4 km reservoir depth. Thermal model uses a 1×1 km reservoir (3.14 km^3 volume) and the simulations are truncated at 60% crystallinity. Red dashed lines highlight 10 and 20 MPa overpressure thresholds (see discussion). b) Thermal model outputs showing temperature variations for the 0.90 X_{H_2O} case after 1 ka, 3 ka and 4.8 ka. c) Thermal model outputs showing overpressure variations for the same case. White dashed line shows extent of magma reservoir at 1 ka. Blue space within this outline at 3 ka and 4.8 ka represents uneruptible magma. (For interpretation of the references to colour in this figure legend, the reader is referred to the web version of this article.)

here, although the magnitude of the overpressure reduction varies with magma composition and storage conditions. Fig. 2 demonstrates that reducing initial X_{H_2O} past a certain point – which varies for each system and is composition-dependent – will mean that no positive overpressure is generated via volatile exsolution.

3.1.3. Effect of reservoir compressibility

The compressibility of the rock surrounding a magma reservoir is termed the reservoir compressibility (β_r), and is dependent on reservoir dimensions and the physical properties of the host rock (Wasser et al., 2021). We do not include β_r in our overpressure calculations, as we assume that the crust surrounding our shallow (4 km depth) magma reservoir is rigid. This is a reasonable assumption, as a crustal viscosity of 10^{20} Pa s – which is likely to be appropriate for systems shallower than $\sim 7.5 \text{ km}$ (Townsend et al., 2019) – gives a relaxation timescale of 158 ka. Hence, the host rock crust is effectively rigid over the volatile exsolution timescales reported here. However, taking β_r into account, overpressure can be recalculated using Eq. (2).

$$\Delta P = \Delta V / (V^* (\beta + \beta_r)) \quad (2)$$

Using a β_r value of $2.0 \times 10^{-10} \text{ Pa}^{-1}$ (Wasser et al., 2021) results in an increase in total compressibility (magma plus reservoir), and a decrease in ΔP of 0.5–20 MPa. This comparison is plotted in fig. S5, which demonstrates that trends in overpressure remain the same, despite a decrease in absolute values.

3.2. Thermal modelling

The results presented above show overpressure calculated for an

internally homogenous system, and they do not give any indication of the timescale required to reach peak ΔP values. In this section we present the temporal evolution of overpressure for a small, shallow magma body, using ΔP values which have been averaged over the whole eruptible volume ($<60\%$ crystals) of the reservoir. The rate of cooling is dependent on the thermal conductivity, specific heat and density of the crust, and the latent heat of crystallisation.

3.2.1. Timescales of overpressurisation: varying initial H_2O content

Fig. 3a shows the effect of varying initial H_2O content (no CO_2) on the temporal evolution of average reservoir overpressure for a cylindrical reservoir situated at 4 km depth, with a radius and height of 1000 m. We only consider magma with crystallinity $<60 \text{ vol\%}$ in our plots. The highest average reservoir overpressure is attained in the simulation which is initially H_2O saturated (3.4 wt%), reaching a peak of 61 MPa after $\sim 3 \text{ Ka}$. The initially fluid undersaturated simulations (2.5 and 2.9 wt% H_2O) show a phase of net underpressurisation, due to prolonged periods of crystallisation in the absence of a fluid phase. After several ka, average reservoir overpressure in the initially undersaturated simulations begins to increase due to fluid exsolution, and eventually positive overpressures are attained. This contrasts with the initially fluid oversaturated simulations (3.9 and 4.3 wt% H_2O), which do not generate any net underpressure, and show a relatively steady average reservoir overpressure increase. There is a clear contrast in the rate of average reservoir overpressure increase between the initially undersaturated and oversaturated simulations. Although the lower H_2O scenarios take longer to reach a given overpressure (e.g. 10 MPa), they show more rapid rates of overpressurisation (e.g. up to 50 MPa in $\sim 0.5 \text{ ka}$ for the 2.9 wt% example). In contrast, the higher H_2O cases reach 10 MPa more rapidly, but show a much slower rate of overpressurisation (e.g.

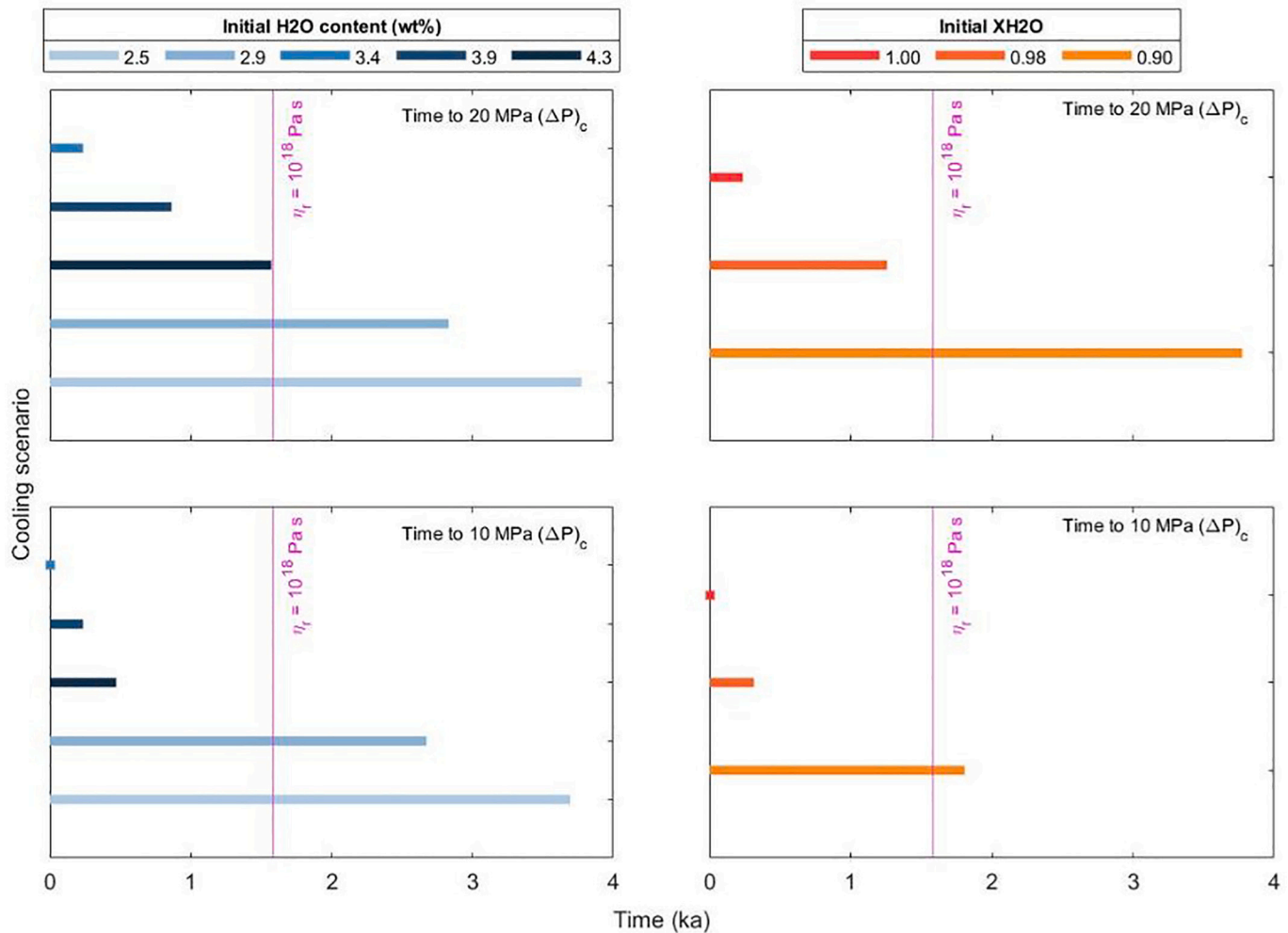


Fig. 5. Summary of the time taken to reach critical overpressures of 20 MPa (top row) and 10 MPa (bottom row) for the scenarios shown in Figs. 3 and 4. Left side shows varying initial H_2O content, right side shows varying initial X_{H_2O} . Note that the 0.5 and 0.7 X_{H_2O} scenarios shown in Fig. 4 do not generate any positive overpressure, so are not shown here. A relaxation timescale (T_{relax}) of 1.58 ka is shown by the pink line, which assumes a crustal viscosity of $10^{18} \text{ Pa s}^{-1}$ (Townsend et al., 2019). Using a crustal viscosity of $10^{19} \text{ Pa s}^{-1}$, which is more realistic for the small, shallow system modelled here, gives a relaxation timescale of 15.8 ka. (For interpretation of the references to colour in this figure legend, the reader is referred to the web version of this article.)

requiring ~ 3 ka to build up 40 MPa of overpressure for the 3.9 wt% H_2O case).

Figs. 3b and c show the spatial evolution of temperature and overpressure within the cooling reservoir for the 3.4 wt% H_2O case. As we apply a crystallinity cut-off of 60 vol%, the volume of the eruptible magma decreases with time, as no recharge events are considered. The spatial distribution of overpressure is governed by the overpressure-temperature relationship shown in Fig. 1c, whereby overpressure increases during cooling, until it reaches a peak at 1020°C , then begins to decrease again as expansion due to fluid exsolution is outweighed by crystallisation contraction. After 1 ka, the interior of the reservoir is still relatively hot, resulting in lower overpressures than those at the outer edge of the reservoir, which has cooled sufficiently to generate peak overpressures. By 3 ka, the peak overpressure ‘front’ has shifted towards the centre of the reservoir, whilst the outer edge has cooled past peak overpressure, and the centre is still increasing in temperature. After 4.8 ka of cooling, the volume of eruptible magma has decreased, and the highest overpressure occurs in the centre of the reservoir.

3.2.2. Timescales of overpressurisation: varying initial X_{H_2O}

Fig. 4a shows the effect of varying initial X_{H_2O} content on the temporal evolution of average reservoir overpressure. Parameters are the same as in section 3.2.1, and the $X_{H_2O} = 1$ case is the same as the 3.4 wt

% H_2O case presented in Fig. 3a. Magma with $X_{H_2O} = 1$ generates the greatest average reservoir overpressure, and overpressure decreases as X_{H_2O} decreases. Maximum average reservoir overpressure is 61 MPa for $X_{H_2O} = 1$, and decreases to 42 MPa for $X_{H_2O} = 0.98$ and 23 MPa for $X_{H_2O} = 0.90$. The $X_{H_2O} = 0.70$ and 0.50 cases do not generate any positive average reservoir overpressure due to the effect of CO_2 described in section 4.2. The rate of average reservoir overpressure build-up also decreases with decreasing X_{H_2O} . For example, the $X_{H_2O} = 1$ case reaches 20 MPa in ~ 0.2 ka, whilst the $X_{H_2O} = 0.90$ simulation reaches 20 MPa in ~ 3.8 ka. Figs. 4b and c show the spatial evolution of temperature and overpressure within the cooling reservoir for the 0.90 X_{H_2O} case. This is governed by the overpressure-temperature profile shown in Fig. 2c, which demonstrates that the highest overpressures for this scenario occur above 60 vol% crystallinity. For this reason, the highest overpressure always occurs at the cooling edge of the reservoir, at high crystallinities and moves inwards as the eruptible volume decreases.

4. Discussion

4.1. Critical overpressures and timescales of pressurization

To assess whether volatile exsolution is a viable eruption trigger for the different cases we have investigated, we frame our results in the

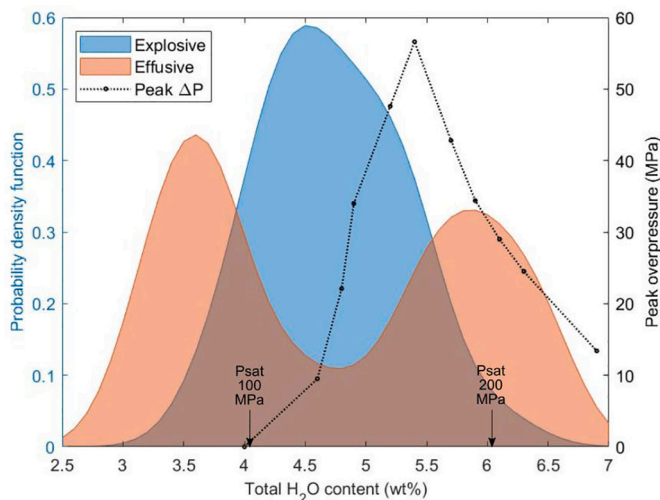


Fig. 6. Magmatic H_2O content, eruption style and peak overpressure. Shaded areas show kernel density estimation for H_2O content/ eruption style data from Popa et al. (2021b), which comprises global data from 245 eruptions from 75 volcanoes. Black dashed line shows peak overpressure from Rhyolite-MELTS modelling for Nisyros-Yali. Arrows show H_2O contents corresponding to saturation pressures (P_{sat}) of 100 and 200 MPa, a common magma reservoir pressure range. P_{sat} is determined using Volatilecalc (Newman and Lowenstern, 2002), for rhyolitic melt at 800 °C.

context of a critical overpressure (ΔP_c). Most researchers define failure as possible when overpressure exceeds twice the tensile strength (T_s) of the host rock (Tait et al., 1989; Parfitt et al., 1993). A reasonable estimate of T_s for volcanic rocks is 5–10 MPa (Gudmundsson, 2011; Albino et al., 2018), giving a critical overpressure range of 10–20 MPa, which we adopt here. We note that, in natural systems, the presence of fractures in the host rock will result in a reduction in T_s , and therefore also in (ΔP_c) (Zhan and Gregg, 2019).

For volatile-exsolution to trigger an eruption, overpressure build-up must occur on a timescale shorter than that of crustal relaxation. The average reservoir overpressure timescales shown in Figs. 3 & 4 can be compared to timescales of viscous crustal relaxation (τ_{relax}) to determine whether they are fast enough to potentially trigger an eruption. τ_{relax} can be calculated from the equation of Degruyter and Huber (2014):

$$\tau_{relax} = \eta r / (\Delta P_c) \quad (2)$$

Where ηr is host rock viscosity. Using $\eta r = 10^{19}$ Pa s (Townsend et al., 2019) and (ΔP_c) = 20 MPa gives a crustal relaxation timescale of 15.8 ka. Using a host rock viscosity of 10^{18} Pa s, representing warmer crust, gives $\tau_{relax} = 1.6$ ka, whilst increasing ηr to 10^{20} Pa s, representing cooler crust, gives $\tau_{relax} = 158$ ka. For the reservoir at 4 km depth modelled here, higher viscosities and therefore longer relaxation timescales may be more appropriate. However, for long-lived, larger and deeper systems, considering the effect of periodic magma recharge on the heat budget of the upper crustal reservoir (e.g. Annen et al., 2015), τ_{relax} may be equal to or shorter than the cooling and overpressurisation timescale. Fig. 3 shows that all the modelled scenarios reach a critical overpressure of 10 MPa well within a relaxation timescale of 15.8 ka. If a more conservative τ_{relax} of 1.6 ka is used, the 3.4–4.3 wt% H_2O simulations still have the potential to trigger an eruption, whilst the initially H_2O -undersaturated simulations do not, as they exsolve fluids more slowly than τ_{relax} . These H_2O -undersaturated scenarios display periods of average underpressurisation over several ka, but once fluids begin to exsolve overpressure increases rapidly over ~ 0.5 ka. For the mixed H_2O - CO_2 scenarios shown in Fig. 4, magmas with initial $X_{H_2O} \geq 0.90$ reach 10 MPa within a τ_{relax} of 15.8 ka, and those with $X_{H_2O} \geq 0.98$ reach 10 MPa using a more conservative τ_{relax} of 1.6 ka. A summary of the timescales taken to reach critical overpressures of 10 and 20 MPa, for a

reservoir volume of 3.14 km³, is shown in Fig. 5. This highlights that eruption triggering via volatile-exsolution becomes less likely as initial magmatic X_{H_2O} decreases. It also demonstrates that magmas with higher X_{H_2O} values can attain critical overpressures on timescales $< \tau_{relax}$, even when using conservative τ_{relax} estimates which are likely to be more characteristic of deeper, hotter (lower viscosity) systems. The effect of varying reservoir volume on timescales to reach critical overpressure is shown in Fig. S6. This demonstrates the sensitivity of overpressure build-up not only to reservoir volume, but also to initial H_2O content and fluid composition.

For cases where peak overpressure is attained after reaching 60% crystallinity, the highest overpressures are confined to the cooling edge of the reservoir, and decrease inwards (Fig. 4c). However, if peak overpressure is attained prior to reaching 60% crystallinity, high overpressures are not only restricted to the edge of the cooling magma body, they can also develop within the reservoir (Fig. 3c). Our results demonstrate that volatile-exsolution driven overpressure can attain critical magnitudes on timescales shorter than that of crustal relaxation, when considering small reservoirs situated at shallow depths. The lack of convective heat transfer in our thermal model means that the timescales presented here are likely to be maximum estimates, as the presence of a hydrothermal system can increase the rate of heat loss by an order of magnitude (Kelly et al., 2021), though this is also dependent on reservoir size.

4.2. Implications for eruption triggering

When we vary the CO_2 content of our mixed fluid simulations, we find that overpressure increases as X_{H_2O} increases (Figs. 2 & 4). The reduction in overpressure with decreasing X_{H_2O} occurs because CO_2 is less soluble than H_2O at shallow magma storage depths. As X_{H_2O} decreases, the volume of exsolved fluids at the liquidus increases – and this results in a smaller volumetric expansion relative to simulations with higher X_{H_2O} (see Fig. S7). In addition, simulations with a greater proportion of CO_2 (lower X_{H_2O}) initially have higher compressibilities due to their greater volumes of exsolved fluids (H_2O and CO_2), and tendency to exsolve fluids earlier. This results in lower overpressures relative to simulations with higher X_{H_2O} . This is consistent with Tait et al. (1989), who identified that more soluble volatile species (i.e. H_2O) play a greater role in overpressure generation. Once initial X_{H_2O} is reduced below a certain point, the system does not generate any positive overpressure during cooling, limiting the potential for eruption triggering via volatile exsolution. At Kelud, Cassidy et al. (2019) identified variations in X_{H_2O} and potential triggering mechanism. The 2007 effusive eruption was associated with low X_{H_2O} values (~ 0.55), and was preceded by influx of a CO_2 -rich magma, which triggered the eruption. In contrast, the explosive eruption in 2014 was characterized by higher X_{H_2O} values (~ 1.00) and is thought to have been triggered by second boiling. Our thermal modelling results show that average reservoir overpressures of 10s of MPa can be generated with magmatic X_{H_2O} of 0.90–1.00 (Fig. 4a). In contrast, our simulations with X_{H_2O} values ≤ 0.70 do not generate any positive overpressure during cooling. This supports the idea that volatile exsolution was a possible trigger for the explosive 2014 eruption, whilst it is an unlikely trigger for the 2007 eruption – instead requiring an alternative triggering mechanism, such as magma injection. If this is the case, then (ΔP_c) for the 2014 eruption must have been attained within seven years (the time interval between the two eruptions). As shown in Fig. 4a, average reservoir overpressure for our $X_{H_2O} = 1$ case can build to critical levels of 10 MPa rapidly. However, the timescales presented here are not as rapid as those seen in some real volcanic systems. This discrepancy is likely to occur because, in reality, volcanoes operate as open-systems. At Kelud, open system behaviour is evidenced by the large volumes of CO_2 which were outgassed during the 2007 eruption (Caudron et al., 2012). This linking of the magmatic system with its exterior is likely to accelerate cooling rates. In addition, it is also likely that heat loss by convection would occur in real volcanic systems, and

this would accelerate the cooling process. We reiterate that we are presenting general trends in overpressure timescales, and that incorporating convection into our modelling would shorten our timescale estimates.

Our cooling reservoir model shows the decrease in eruptible reservoir volume with time as magma cools below the 60 vol% crystallinity cut-off (Figs. 3c and 4c). Eruptions generated by magmas which take longer to attain critical overpressure may have smaller volumes, as there is less eruptible magma in the reservoir (assuming no recharge). In contrast, eruptions which attain critical overpressure earlier in their cooling history may be more voluminous, as there is a greater volume of potentially eruptible magma in the reservoir. For example, the 3.4 wt% H₂O scenario (initially at the H₂O solubility limit) shown in Fig. 3 has an eruptible volume of 2.3 km³ by the time it attains 20 MPa of average reservoir overpressure after ~0.16 ka. In contrast, the 4.3 wt% H₂O magma (initially H₂O-oversaturated) has an eruptible volume of 1.2 km³ when it reaches 20 MPa at ~1.6 ka. For the 2.5 wt% H₂O magma (initially H₂O-undersaturated) the eruptible volume is reduced to 0.30 km³ once it reaches the same critical overpressure after ~3.7 ka.

We focus on the role of initial fluid content, with no external addition of magma or fluids. However, flushing of a reservoir by CO₂-rich fluids can also result in reservoir pressurization, provided that flushing occurs prior to rheological lock-up (Caricchi et al., 2018). CO₂ flushing into the reservoir may increase magma compressibility, but if this is rapid and voluminous enough, it will still meet the overpressure threshold for triggering an eruption. For flushing to trigger an eruption for the cases considered here, the supply of CO₂-rich fluids has to occur on a timescale shorter than τ_{relax} , and also shorter than the exsolution-driven overpressurisation timescale. This process of CO₂ flushing is distinct from the role of CO₂ exsolution described here, where the lower solubility of this phase has less intrinsic overpressure generating potential when compared to H₂O.

4.3. Implications for eruption style

Our modelling shows that magmas generate the greatest exsolution-driven overpressures when their initial H₂O contents are at the solubility limit (figs 1 & 3). Reducing H₂O content so that the magma is initially undersaturated reduces potential volume change, resulting in a reduction in overpressure. Increasing the initial H₂O content, so that the magma is initially water-oversaturated, results in an increase in compressibility and a reduction in overpressure due to the ability of exsolved fluids to accommodate pressure increase (Woods and Pyle, 1997; Popa et al., 2021b). This variation in overpressure-generating capacity with varying fluid content may have implications for magma ascent rate and eruption style. Whilst it is well-established that ascent rate is a major control on eruption style (Cassidy et al., 2018), the factors controlling initial ascent rate are debated. One of the proposed controls is magma reservoir overpressure (Jaupart and Allègre, 1991). Indeed, conduit flow models show that increasing magmatic overpressure results in faster initial ascent speeds (Woods and Koyaguchi, 1994; Thomas and Neuberg, 2014). Popa et al. (2021b) compiled global magmatic H₂O contents and found that magmas close to their water solubility limit are associated with explosive eruptions, whilst effusive eruptions are more commonly linked to either very high or low H₂O contents (albeit with crystallinity also as a factor). This compilation of magma H₂O content, separated by eruption style, is shown alongside peak overpressure from our Rhyolite-MELTS simulations in Fig. 6, where we propose a potential link between overpressure and eruption style. The high overpressures seen at the solubility limit broadly correlate with the distribution of pre-eruptive H₂O contents of explosive eruptions. We propose that the high overpressures at the volatile 'sweet spot' may be contributing to faster initial ascent rates and therefore to more explosive eruptions. In contrast, the reduction in overpressure with increasing or decreasing H₂O could potentially lower ascent rates, favouring effusive eruptions. This may provide another, concurrent mechanism for the

abundance of water-rich effusive events, in addition to the effect of exsolved volatiles on melt viscosity and reservoir reheating upon recharge, and the effect of exsolved volatiles present during early conduit ascent, as described in Popa et al. (2021b).

Our findings do not account for the occurrence of explosive volatile-over saturated eruptions. High magmatic H₂O contents increase magma compressibility, resulting in lower reservoir overpressures. Whilst this makes eruption triggering less likely, if these magmas do erupt their increased buoyancy and low viscosity may increase ascent rate, promoting an explosive eruption (La Spina et al., 2022). This suggests that processes operating during magma ascent may in some instances modify and 'override' the effects of overpressurisation in the reservoir. Alternatively, high levels of exsolved volatiles in magmas may increase permeability during ascent, favouring gas loss and promoting an effusive eruption (Popa et al., 2021b). Studies which couple models of reservoir overpressurisation with ascent rate and fragmentation - especially focusing on volatile content, crystallinity, viscosity and buoyancy - would help to advance our understanding of the many factors which contribute to volcanic eruption style.

5. Potential model limitations

5.1. Pressure dissolution

The assumption of a rigid crust surrounding the magma reservoir means that any overpressure generated by cooling and crystallisation cannot be dissipated by expansion of the host rock. This build-up of ΔP will affect the solubility of volatiles in the system, potentially resulting in volatile redissolution and system volume decrease. In turn, this may also affect the liquid composition and crystallinity of the magma. To investigate the effect of overpressurisation on fluid solubility further, we run MELTS simulations where the overpressure generated in the previous step is added on to the lithostatic pressure. We do this for temperature intervals of 0.5 °C, and do not allow reservoir pressure to drop below 100 MPa (the initial lithostatic pressure used in the isobaric simulations).

Fig. S8 shows that incorporating overpressure into the simulations results in multiple cycles of under- and overpressurisation. For example, adding on 6 MPa of exsolution-driven overpressure (fig. S8a) results in a reservoir pressure of 106 MPa. Running a simulation at this increased reservoir pressure (106 MPa) leads to a melt density increase, and redissolution of exsolved volatiles as solubility is increased at higher pressure. Both of these factors lead to a volume decrease relative to the initial volume at 100 MPa, resulting in underpressurisation of -17 MPa. This then reduces the reservoir pressure for the next set of simulations, which are run at 100 MPa, leading to fluid exsolution, volume increase and overpressurisation to 16 MPa. This results in another cycle of fluid dissolution, this time at a higher reservoir pressure of 116 MPa. The system continues to swing between these two states of increased and decreased pressure. Although the overpressure profiles are altered, the relative magnitudes for the varying $X_{\text{H}_2\text{O}}$ simulations are similar to their isobaric counterparts. Fig. S8 suggests that timescales to reach critical overpressures may be altered when fluctuations due to overpressurisation are accounted for. However, it is difficult to quantify this as the fluctuations in crystallinity as pressure changes mean this cannot be input into the thermal model. Our model is therefore limited for simulating the effect of system change due to incremental, non-isobaric overpressure increase, and is unlikely to reflect the full complexity of a natural system.

5.2. Closed system assumption

When calculating overpressure we assume a closed system, where all exsolved fluids are retained within the magma reservoir. This is a common assumption when modelling magmatic systems (e.g., Gleeson et al., 2017; Tramontano et al., 2017; Caricchi et al., 2018), but it is at

odds with observations of volcanic degassing. However, numerical modelling of bubble migration in melts has shown that the majority of outgassing ($\sim 50\%$ of the available fluid phase) occurs at medium to high crystallinities of 40–70%, with only $\sim 1\%$ of fluids lost at crystallinities $<40\%$ (Parmigiani et al., 2017; Degruyter et al., 2019). At crystallinities $<40\%$, bubble migration is inefficient, and only a very small volume of gas is lost this way. For the cases presented here, all of the scenarios shown in Fig. 3a reach 20 MPa critical overpressure prior to attaining 40% crystallinity. This can effectively be considered as a closed system, as fluid loss during this time will be negligible. However, whilst the $X_{\text{H}_2\text{O}} = 1$ and 0.98 cases shown in Fig. 4a also attain $(\Delta P)_c$ prior to 40% crystallinity, the lower $X_{\text{H}_2\text{O}}$ cases ($\leq 0.90 X_{\text{H}_2\text{O}}$) do not. For example, the 0.90 $X_{\text{H}_2\text{O}}$ scenario attains $(\Delta P)_c$ at a crystallinity of $\sim 50\%$. This suggests that the closed system assumption may not be valid for the lower $X_{\text{H}_2\text{O}}$ scenarios presented here, as significant amounts of degassing via fluid pathways begins to play a role prior to attaining $(\Delta P)_c$.

To quantify the effect of gas loss from the reservoir, we remove 10% of the available exsolved fluid volume at 50% crystallinity, and recalculate the system volume, compressibility, and overpressure accordingly. We use the 50% crystallinity interval as this is within the high outgassing range specified in Parmigiani et al. (2017), as outlined above, and we use 10% fluid loss as an arbitrary volume, to illustrate the effect of open-system degassing. Fig. 7 shows that, for the open system model, overpressures (at 50% crystallinity) are reduced by ~ 4 –10 MPa when 10% of the available fluids are lost from the system. Although overpressure is reduced across all the simulations, the trend in overpressure with varying fluid content is the same as in the closed system simulations. This reduction in overpressure due to gas loss means that open systems may take longer to reach critical overpressures than those with no gas loss. Although, as outlined above, this will only be relevant for systems where $(\Delta P)_c$ is attained after reaching $\sim 40\%$ crystallinity.

6. Conclusions

Our thermodynamic modelling demonstrates that magmas with H_2O contents at their solubility limit, and those with low CO_2 contents, generate the highest exsolution-driven overpressures and have the greatest potential for internal eruption triggering (figs1 & 2). When

coupled to a thermal model, we show that overpressurisation to critical values can be achieved well within typical relaxation timescales, for small and shallow magma reservoirs (Figs. 3, 4 & 5). For CO_2 -free scenarios, the greatest rates of overpressure increase are seen in magmas which are initially H_2O -undersaturated. As initial H_2O content increases, the rate of overpressure build-up is reduced (Fig. 3a). For the mixed H_2O - CO_2 scenarios, rate of overpressurisation decreases as $X_{\text{H}_2\text{O}}$ decreases. The reduction in overpressure with decreasing magmatic $X_{\text{H}_2\text{O}}$ suggests that, below a certain point, volatile-exsolution is not a viable eruption triggering mechanism (Fig. 4a). We propose that the variation in overpressure with initial H_2O content may be one factor affecting magma ascent rate and explosivity (Fig. 6). Peak overpressures at the volatile ‘sweet spot’ may drive faster ascent rates, which, combined with other factors, allows less time for volatile outgassing and ultimately favours fragmentation and explosive eruptions. At low H_2O contents, magmas have a reduced potential for volumetric expansion, whilst high H_2O contents induce fluid exsolution and increase system compressibility – both of these factors reduce overpressure and make eruption triggering via volatile-exsolution less likely.

By coupling thermodynamic and thermal models we provide a novel method for tracking overpressure within a cooling magma reservoir. However, we also note that our method does not account for the effect of cooling via convection, which in reality would reduce our time to critical overpressure. We also do not account for the effect of changes in pressure on volatile solubility. Accurate modelling of the feedbacks between crustal response and magma thermodynamics is an area of research which would greatly improve our understanding of overpressurisation. The temporal variations in overpressure presented here could be used as inputs for dyke propagation models, which often assume a constant reservoir overpressure (Rivalta et al., 2015). Our methodology could also be used to link reservoir processes with time series of precursory volcanic activity, or to conduit models, where overpressure, volatile content, crystallinity and viscosity are important factors. Our results have implications for volcano monitoring, suggesting that elucidation of magma overpressures via ground deformation and numerical modelling (Masterlark et al., 2016; Bato et al., 2017) may be a promising way to forecast explosive eruptions.

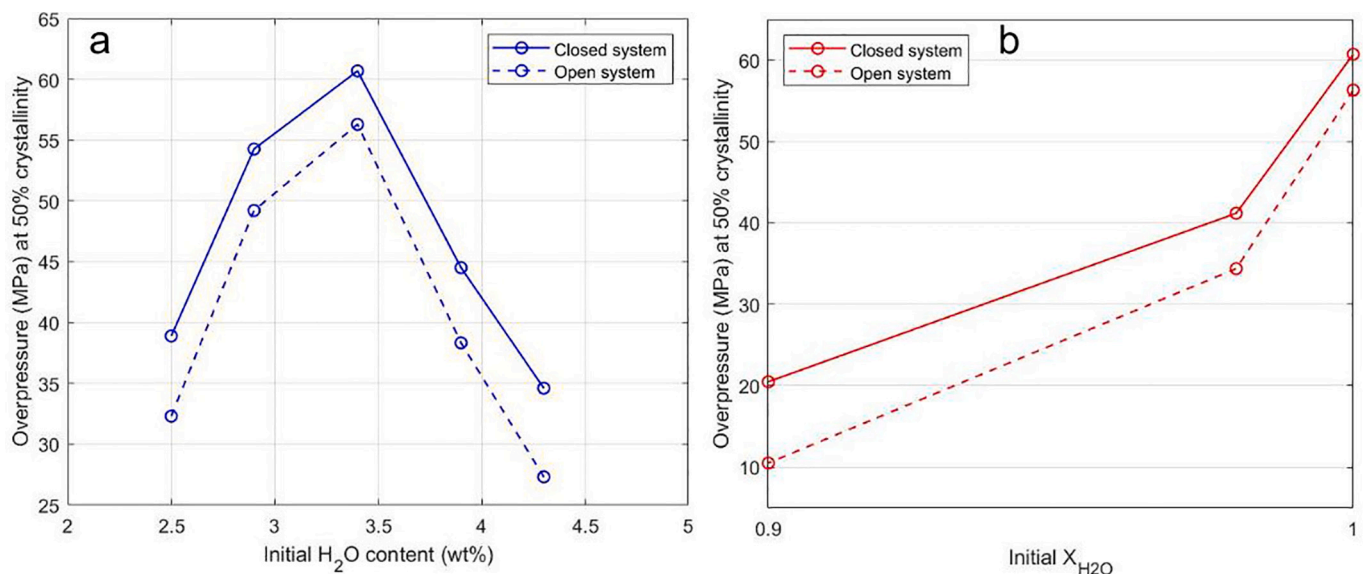


Fig. 7. Comparing the effect of open- versus closed-system behaviour on overpressure magnitude for a) varying initial H_2O content, and b) varying initial $X_{\text{H}_2\text{O}}$. Both examples using Kelud (100 MPa). The closed-system results are the same as those shown in Figs. 1c and 2c, where all fluids are retained within the system. The open-system results were calculated by subtracting 10% of the exsolved fluid volume at 50% crystallinity. The system volume and compressibility are then adjusted accordingly, and overpressure is recalculated based on the new values.

CRedit authorship contribution statement

Anna Brookfield: Conceptualization, Methodology, Formal analysis, Investigation, Writing – original draft, Visualization. **Mike Cassidy:** Conceptualization, Methodology, Writing – review & editing, Supervision. **Gregor Weber:** Conceptualization, Methodology, Software, Writing – review & editing. **Răzvan-Gabriel Popa:** Conceptualization, Writing – review & editing. **Olivier Bachmann:** Conceptualization, Writing – review & editing. **Michael J. Stock:** Writing – review & editing.

Declaration of Competing Interest

None.

Data availability

Data will be made available on request.

Acknowledgements

This research was funded by a Natural Environmental Research Council (NERC) Doctoral Training Partnership studentship to Anna Brookfield (NE/L002612/1). G.W. acknowledges funding through an early postdoc mobility fellowship (project number: P2GEP2 195238) from the Swiss National Science Foundation. M.C. acknowledges a NERC fellowship (NE/N014286/1).

Appendix A. Supplementary data

Supplementary data to this article can be found online at <https://doi.org/10.1016/j.jvolgeores.2023.107916>.

References

- Albino, F., Amelung, F., Gregg, P., 2018. The Role of Pore Fluid pressure on the failure of Magma Reservoirs: Insights from Indonesian and Aleutian Arc Volcanoes. *J. Geophys. Res. Solid Earth* 123 (2). <https://doi.org/10.1002/2017JB014523>.
- Annen, C., Burgisser, A., 2021. Modeling water exsolution from a growing and solidifying felsic magma body. *Lithos* 402–403. <https://doi.org/10.1016/j.lithos.2020.105799>.
- Annen, C., Blundy, J.D., Sparks, R.S.J., 2006. The genesis of intermediate and silicic magmas in deep crustal hot zones. *J. Petrol.* 47 (3) <https://doi.org/10.1093/petrology/egi084>.
- Annen, C., et al., 2015. Construction and evolution of igneous bodies: Towards an integrated perspective of crustal magmatism. *Lithos*. <https://doi.org/10.1016/j.lithos.2015.05.008>.
- Azzilli, F., et al., 2019. The unexpected explosive sub-Plinian eruption of Calbuco volcano (22–23 April 2015; southern Chile): Triggering mechanism implications. *J. Volcanol. Geotherm. Res.* 378 <https://doi.org/10.1016/j.jvolgeores.2019.04.006>.
- Bato, M.G., Pintel, V., Yan, Y., 2017. Assimilation of deformation data for eruption forecasting: potentiality assessment based on synthetic cases. *Front. Earth Sci.* 5 <https://doi.org/10.3389/feart.2017.00048>.
- Blake, S., 1984. Volatile oversaturation during the evolution of silicic magma chambers as an eruption trigger. *J. Geophys. Res.* 89 (B10) <https://doi.org/10.1029/JB089iB10p08237>.
- Cañón-Tapia, E., 2014. Volcanic eruption triggers: a hierarchical classification. *Earth Sci. Rev.* 129, 100–119. <https://doi.org/10.1016/j.earscirev.2013.11.011>.
- Caricchi, L., et al., 2014. Frequency and magnitude of volcanic eruptions controlled by magma injection and buoyancy. *Nat. Geosci.* 7 (2), 126–130. <https://doi.org/10.1038/ngeo2041>.
- Caricchi, L., Sheldrake, T.E., Blundy, J., 2018. Modulation of magmatic processes by CO₂ flushing. *Earth Planet. Sci. Lett.* 491 <https://doi.org/10.1016/j.epsl.2018.03.042>.
- Cashman, K.V., 2004. Volatile controls on magma ascent and eruption. In: *The State of the Planet: Frontiers and Challenges in Geophysics*. Geophysical Monograph Series. International Union of Geodesy and Geophysics and the American Geophysical Union. <https://doi.org/10.1029/150GM10>.
- Cassidy, M., et al., 2016. Volatile dilution during magma injections and implications for volcano explosivity. *Geology* 44 (12). <https://doi.org/10.1130/G38411.1>.
- Cassidy, M., et al., 2018. Controls on explosive-effusive volcanic eruption styles. *Nat. Commun.* 9 (1) <https://doi.org/10.1038/s41467-018-05293-3>.
- Cassidy, M., et al., 2019. Explosive eruptions with little warning: experimental petrology and volcano monitoring observations from the 2014 eruption of Kelud, Indonesia. *Geochim. Geophys. Res.* <https://doi.org/10.1029/2018gc008161>.
- Caudron, C., Mazot, A., Bernard, A., 2012. Carbon dioxide dynamics in Kelud volcanic lake. *J. Geophys. Res. Solid Earth*. <https://doi.org/10.1029/2011JB008806>.
- Cooper, K.M., Kent, A.J.R., 2014. Rapid remobilization of magmatic crystals kept in cold storage. *Nature* 506 (7489), 480–483. <https://doi.org/10.1038/nature12991>.
- Degruyter, W., Huber, C., 2014. A model for eruption frequency of upper crustal silicic magma chambers. *Earth Planet. Sci. Lett.* 403 <https://doi.org/10.1016/j.epsl.2014.06.047>.
- Degruyter, W., et al., 2019. How do volatiles escape their shallow magmatic hearth? *Phil. Trans. R. Soc. A Math. Phys. Eng. Sci.* 377 (2139) <https://doi.org/10.1098/rsta.2018.0017>.
- Ghiorso, M.S., Gualda, G.A.R., 2015. An H₂O–CO₂ mixed fluid saturation model compatible with rhyolite-MELTS. *Contrib. Mineral. Petrol.* 169 (6) <https://doi.org/10.1007/s00410-015-1141-8>.
- Gleeson, M.L.M., et al., 2017. Constraining magma storage conditions at a restless volcano in the Main Ethiopian Rift using phase equilibria models. *J. Volcanol. Geotherm. Res.* 337 <https://doi.org/10.1016/j.jvolgeores.2017.02.026>.
- Gonnermann, H.M., Manga, M., 2012. Dynamics of magma ascent in the volcanic conduit. In: Fagots, S.A., Gregg, T.K.P., Lopes, R.M.C. (Eds.), *Modeling Volcanic Processes: The Physics and Mathematics of Volcanism*. Cambridge University Press. <https://doi.org/10.1017/CBO9781139021562.004>.
- Gottsmann, J., Odbert, H., 2014. The effects of thermomechanical heterogeneities in island arc crust on time-dependent pre-eruptive stresses and the failure of an andesitic reservoir. *J. Geophys. Res. Solid Earth* 119 (6), 4626–4639. <https://doi.org/10.1002/2014JB011079>.
- Gregg, P.M., et al., 2012. Catastrophic caldera-forming eruptions: Thermomechanics and implications for eruption triggering and maximum caldera dimensions on Earth. *J. Volcanol. Geotherm. Res.* 241–242. <https://doi.org/10.1016/j.jvolgeores.2012.06.009>.
- Grosfils, E.B., et al., 2015. Elastic models of magma reservoir mechanics: a key tool for investigating planetary volcanism. *Geol. Soc. Spec. Publ.* 401 <https://doi.org/10.1144/SP401.2>.
- Gualda, G.A.R., Ghiorso, M.S., 2015. MELTS Excel: A Microsoft Excel-based MELTS interface for research and teaching of magma properties and evolution, pp. 315–324. <https://doi.org/10.1002/2014GC005545>. Received.
- Gualda, G.A.R., et al., 2012. Rhyolite-MELTS: a modified calibration of MELTS optimized for silica-rich, fluid-bearing magmatic systems. *J. Petrol.* 53 (5) <https://doi.org/10.1093/petrology/egr080>.
- Gudmundsson, A., 2012. Magma chambers: Formation, local stresses, excess pressures, and compartments. *J. Volcanol. Geotherm. Res.* 237–238, 19–41. <https://doi.org/10.1016/j.jvolgeores.2012.05.015>. Elsevier B.V.
- Huber, C., et al., 2019. Optimal depth of subvolcanic magma chamber growth controlled by volatiles and crust rheology. *Nat. Geosci.* 12 (9) <https://doi.org/10.1038/s41561-019-0415-6>.
- Huppert, H.E., Woods, A.W., 2002. The role of volatiles in magma chamber dynamics. *Nature* 420 (6915), 493–495. <https://doi.org/10.1038/nature01211>. Nature Publishing Group.
- Jaupart, C., Allègre, C.J., 1991. Gas content, eruption rate and instabilities of eruption regime in silicic volcanoes. *Earth Planet. Sci. Lett.* 102 (3–4) [https://doi.org/10.1016/0012-821X\(91\)90032-D](https://doi.org/10.1016/0012-821X(91)90032-D).
- Kelly, L.J., et al., 2021. Hydrothermal cooling as a requirement for short storage of silicic magmas. *Geochim. Geophys. Res.* 22 (9) <https://doi.org/10.1029/2021GC009794>.
- Kent, A.J.R., et al., 2007. Vapor transfer prior to the October 2004 eruption of Mount St. Helens, Washington. *Geology* 35 (3). <https://doi.org/10.1130/G22809A.1>.
- Kent, A.J.R., et al., 2010. Preferential eruption of andesitic magmas through recharge filtering. *Nat. Geosci.* 3 (9) <https://doi.org/10.1038/ngeo924>.
- Klein, J., Mueller, S.P., Castro, J.M., 2017. The influence of crystal size distributions on the rheology of magmas: new insights from analog experiments. *Geochim. Geophys. Res.* 18 (11) <https://doi.org/10.1002/2017GC007114>.
- La Spina, G., et al., 2022. Role of volatiles in highly explosive basaltic eruptions. *Nat. Commun.* 3 (156) <https://doi.org/10.1038/s43247-022-00479-6>. Springer US.
- Masterlark, T., et al., 2016. Volcano deformation source parameters estimated from InSAR: Sensitivities to uncertainties in seismic tomography. *J. Geophys. Res. Solid Earth* 121 (4). <https://doi.org/10.1002/2015JB012656>.
- Papale, P., Neri, A., MacEdonio, G., 1998. The role of magma composition and water content in explosive eruptions. 1. Conduit ascent dynamics. *J. Volcanol. Geotherm. Res.* 87 (1–4) [https://doi.org/10.1016/S0377-0273\(98\)00101-2](https://doi.org/10.1016/S0377-0273(98)00101-2).
- Parmigiani, A., et al., 2017. The mechanics of shallow magma reservoir outgassing. *Geochim. Geophys. Res.* 18 (8) <https://doi.org/10.1002/2017GC006912>.
- Pollard, D.D., 1987. Elementary fracture mechanics applied to the structural interpretation of dykes. In: Halls, H., Fahrig, W. (Eds.), *Mafic Dyke Swarms*, 34th edn. Geological Association of Canada, pp. 5–24.
- Popa, R.G., et al., 2019. A connection between magma chamber processes and eruptive styles revealed at Nisyros-Yali volcano (Greece). *J. Volcanol. Geotherm. Res.* 387 <https://doi.org/10.1016/j.jvolgeores.2019.106666>.
- Popa, R.G., Bachmann, O., Huber, C., 2021a. Explosive or effusive style of volcanic eruption determined by magma storage conditions. *Nat. Geosci.* 14 (10), 781–786. <https://doi.org/10.1038/s41561-021-00827-9>. Springer US.
- Popa, R.G., Tolan, P., et al., 2021b. Water exsolution in the magma chamber favors effusive eruptions: Application of Cl-F partitioning behavior at the Nisyros-Yali volcanic area. *Chem. Geol.* 570 <https://doi.org/10.1016/j.chemgeo.2021.120170>.
- Pyle, D.M., Pyle, D.L., 1995. Bubble migration and the initiation of volcanic eruptions. *J. Volcanol. Geotherm. Res.* 67 (4) [https://doi.org/10.1016/0377-0273\(94\)00111-S](https://doi.org/10.1016/0377-0273(94)00111-S).
- Rasmussen, D.J., et al., 2022. Magmatic water content controls the pre-eruptive depth of arc magmas. *Science* 375 (6585). <https://doi.org/10.1126/science.abc5174>.
- Rivalta, E., et al., 2015. A review of mechanical models of dike propagation: Schools of thought, results and future directions. *Tectonophysics* 638, 1–42. <https://doi.org/10.1016/j.tecto.2014.10.003>.

- Rubin, A.M., 1995. Propagation of magma-filled cracks. *Annu. Rev. Earth Planet. Sci.* 23 <https://doi.org/10.1146/annurev.ea.23.050195.001443>.
- Ruprecht, P., Bachmann, O., 2010. Pre-eruptive reheating during magma mixing at Quizapu volcano and the implications for the explosiveness of silicic arc volcanoes. *Geology* 38 (10). <https://doi.org/10.1130/G31110.1>.
- Ruprecht, P., Plank, T., 2013. Feeding andesitic eruptions with a high-speed connection from the mantle. *Nature* 500 (7460). <https://doi.org/10.1038/nature12342>.
- Stock, M.J., et al., 2016. Late-stage volatile saturation as a potential trigger for explosive volcanic eruptions. *Nat. Geosci.* 9 (3) <https://doi.org/10.1038/ngeo2639>.
- Tait, S., Jaupart, C., Vergnolle, S., 1989. Pressure, gas content and eruption periodicity of a shallow, crystallising magma chamber. *Earth Planet. Sci. Lett.* [https://doi.org/10.1016/0012-821X\(89\)90025-3](https://doi.org/10.1016/0012-821X(89)90025-3).
- Thomas, M.E., Neuberg, J.W., 2014. Understanding which parameters control shallow ascent of silicic effusive magma. *Geochem. Geophys. Geosyst.* 15 (11) <https://doi.org/10.1002/2014GC005529>.
- Townsend, M., et al., 2019. Magma chamber growth during intercaldera periods: insights from thermo-mechanical modeling with applications to Laguna del Maule, Campi Flegrei, Santorini, and Aso. *Geochem. Geophys. Geosyst.* 20 (3) <https://doi.org/10.1029/2018GC008103>.
- Tramontano, S., Gualda, G.A.R., Ghiorso, M.S., 2017. Internal triggering of volcanic eruptions: tracking overpressure regimes for giant magma bodies. *Earth Planet. Sci. Lett.* 472, 142–151. <https://doi.org/10.1016/j.epsl.2017.05.014>. Elsevier B.V.
- Trasatti, E., et al., 2019. Magma Degassing as a source of Long-Term Seismicity at Volcanoes: the Ischia Island (Italy) case. *Geophys. Res. Lett.* 46 (24) <https://doi.org/10.1029/2019GL085371>.
- Wasser, V.K., et al., 2021. Multidisciplinary constraints on magma compressibility, the pre-eruptive exsolved volatile fraction, and the H₂O/CO₂ molar ratio for the 2006 Augustine Eruption, Alaska. *Geochem. Geophys. Geosyst.* 22 (9) <https://doi.org/10.1029/2021GC009911>.
- Weber, G., Simpson, G., Caricchi, L., 2020. Magma diversity reflects recharge regime and thermal structure of the crust. *Sci. Rep.* 10 (1) <https://doi.org/10.1038/s41598-020-68610-1>.
- Whittington, A.G., Hofmeister, A.M., Nabelek, P.I., 2009. Temperature-dependent thermal diffusivity of the Earth's crust and implications for magmatism. *Nature* 458 (7236). <https://doi.org/10.1038/nature07818>.
- Woods, A.W., Koyaguchi, T., 1994. Transitions between explosive and effusive eruptions of silicic magmas. *Nature* 370 (6491). <https://doi.org/10.1038/370641a0>.
- Woods, A.W., Pyle, D.M., 1997. The control of chamber geometry on triggering volcanic eruptions. *Earth Planet. Sci. Lett.* 151 (3–4) [https://doi.org/10.1016/S0012-821X\(97\)81845-6](https://doi.org/10.1016/S0012-821X(97)81845-6).